The following publication H. Zhang, L. Bruzzone, W. Shi, M. Hao and Y. Wang, "Enhanced Spatially Constrained Remotely Sensed Imagery Classification Using a Fuzzy Local Double Neighborhood Information C-Means Clustering Algorithm," in IEEE Journal of Selected Topics in Applied Earth Observations and Remote Sensing, vol. 11, no. 8, pp. 2896-2910, Aug. 2018 is available at https://doi.org/10.1109/JSTARS.2018.2846603.

Enhanced Spatially Constrained Remotely Sensed Imagery Classification Using Fuzzy Local Double Neighborhood Information *C*-Means Clustering Algorithm

Hua Zhang, Lorenzo Bruzzone, *Fellow, IEEE,* Wenzhong Shi, Ming Hao, and Yunjia Wang

***Abstract*—This paper presents a fuzzy local double neighborhood information *c*-means (FLDNICM) clustering algorithm for remotely sensed imagery classification which incorporates flexible and accurate local spatial and spectral information. First, a trade-off weighted fuzzy factor is established based on a pixel spatial attraction model that considers spatial distance and class membership differences between the central pixel and its neighbor simultaneously. This factor can adaptively and accurately estimate the spatial constraints from neighboring pixels. To further enhance robustness to noise and outliers, another fuzzy prior probability function is also defined which integrates the mutual dependency information from a pixel and its neighbor in a fuzzy logical way for obtaining accurate spatial contextual information. The FLDNICM enhances the conventional fuzzy *c*-means (FCM) algorithm by producing homogeneous segmentation while reducing the edge blurring artifacts. The new trade-off weighted fuzzy factor and prior probability function are both parameter free and fully adaptive to the image content. Experimental results demonstrate the superiority of FLDNICM over competing methodologies, considering a series of synthetic and real-world images classification applications.**

***Index Terms*—Classification, fuzzy *c*-means clustering, neighborhood, prior probability, remotely sensed imagery.**

I. Introduction

Unsupervised clustering methods for extracting land cover information from remotely sensed imagery are widely used in remote sensing [1]-[5]. Many clustering algorithms and their variations have been exploited for unsupervised classification or segmentation for remote sensing image [2]-[6]. Due to spectral variation, limited spatial resolution and complex spatial arrangement of remotely sensed imagery, a pixel may represent an area on the ground including more than one single land-cover type. Thus, a large amount of imprecise and uncertain pixels may exist in remotely sensed imagery. Fuzzy clustering methods model this uncertainty by allowing pixels to belong to multiple classes with a certain degree of membership. They can also provide a final hard (crisp) map by defuzzification of the pixel membership values. Accordingly, it is natural to apply the concepts of fuzzy set theory to the domain of pixel classification. In this paper, we focus on fuzzy clustering algorithms for unsupervised classification of remotely sensed imagery. One of the popular fuzzy clustering algorithms is the well-known fuzzy *c*-means (FCM) which was first introduced by Dunn [7] and later extended by Bezdek [8]. FCM has robust characteristics for ambiguity and can retain more original image information than hard clustering methods [9]. However, dealing with images corrupted by noise, outliers and other imaging artifacts, the standard FCM often produces clustering maps containing salt and pepper noise [9]-[15]. In addition, the selection of initial cluster centers and cluster number are two problems in FCM [16].

Recently, the issue of incorporating local spatial information into the original FCM to enhance the performance has attracted large interest [9]-[32]. One of the most commonly used methods is to modify the conventional FCM objective function to include the spatial constraints [10]-[26], [28]-[32]. Pham [29] modified the objective function of FCM by including a spatial penalty on the membership functions, which allows the estimation of spatially smooth membership functions. Ahmed *et al.* [13], [28] proposed FCM_S, where a spatial neighborhood term was introduced into the objective function of FCM to compensate for the intensity inhomogeneity. To reduce the computational complexity of FCM_S, Chen and Zhang [30] developed two variants, FCM_S1 and FCM_S2 to simplify the computation of neighborhood term. In order to further speed up the clustering process, Szilagyi *et al.* [31] and Cai *et al.* [14] proposed enhanced FCM (EnFCM) and fast generalized FCM (FGFCM), respectively. However, these extended FCM algorithms perform indirectly on the original image, or need to tune a crucial parameter α for balancing trade-off between the robustness to noise and the effectiveness

Manuscript received 2017; revised 2018; accepted 2018. This work was supported by the National Natural Science Foundation of China under Grant 41331175. (*Corresponding author: Wenzhong Shi*)

H. Zhang is with the School of Environment and Spatial Informatics, China University of Mining and Technology, Xuzhou, 221116, China, and also with the Department of Information Engineering and Computer Science, University of Trento, 38123 Trento, Italy (e-mail: zhhua_79@163.com).

L. Bruzzone is with the Department of Information Engineering and Computer Science, University of Trento, 38123 Trento, Italy (e-mail: lorenzo.bruzzone@ing.unitn.it).

W.Z. Shi is with the Department of Land Surveying and Geo-Informatics, The Hong Kong Polytechnic University, Hung Hom, Kowloon, Hong Kong. (e-mail: lswzshi@polyu.edu.hk).

M. Hao and Y. Wang are with the School of Environment and Spatial Informatics, China University of Mining and Technology, Xuzhou, 221116, China (e-mail: haomingcumt@gmail.com; wyj4139@163.com).

of preserving the image details. This parameter has a crucial impact on the final clustering performance, while its selection is difficult [14], [15]. Moreover, when α is fixed for all neighbor windows across the whole image, it leads to blur the image edges while removing noise.

In order to overcome the above-mentioned limitations, Zhong *et al* [25] provided an adaptive memetic fuzzy clustering algorithm with spatial information for remote sensing imagery (AMASFC), in which the weight of contribution from the spatial neighborhood can be adaptively determined, but the performance improvements in clustering precision are not so impressive. Krinidis and Chatzis [9] proposed a fuzzy local information *c*-means (FLICM), where a fuzzy factor was introduced into the objective function of FCM to guarantee noise insensitiveness and image details preservation. However, this method has some weakness in identifying the class boundary pixels and preserving image details [19]. Gong *et al* [19], [20] further improved FLICM by using a local coefficient of variation to replace the spatial distance as the local similarity measure. Li *et al*. [21] proposed a fuzzy *c*-means with edge and local information (FELICM) based on FLICM to reduce edge degradation. FLICM and above-mentioned enhanced FLICM algorithms are less sensitive to noise to some extent and produce reasonable segmentation maps, whereas the identification of the central pixel is greatly influenced by its neighboring pixels neglecting the central pixel's own features. This results in failing to take full advantage of the information encapsulated in the local window. Moreover, the spatial models used in the clustering procedure are still not as accurate as expected, thus they may fail to correctly distinguish the contributions among neighboring pixels. Accordingly, they may produce over-smooth results for important structures (such as regional borders or edges) and small patches. Furthermore, these methods are not effective when the central pixel is highly different from the neighbor.

To address the aforementioned problems, based on the standard FCM, this paper presents an enhanced FCM named fuzzy local double neighborhood information *c*-means (FLDNICM) clustering algorithm for remotely sensed imagery classification. The aim is to provide a flexible and accurate estimations of spatial constraints on the standard FCM to produce accurate results in homogeneous regions and preserve image details. In contrast with FCM, we consider the classification of a pixel to be influenced by two levels of spatial constraints: spatial continuity and contextual information constraints from neighboring pixels. The main advantages of the FLDNICM algorithm are as follows:

1) Based on the pixel spatial attraction model, proposing a trade-off weighted fuzzy factor to accurately describe the relationships between pixels for retaining edges of regions and small patches when removing noise;

2) Developing a prior probability function by integrating the mutual dependency information from its neighbor in a fuzzy logical way, which a) can enhance the robustness to outliers in a relatively strong noisy environment and b) is able to reduce the edge blurring artifacts when removing isolated pixels;

3) The proposed technique does not require any experimentally adjusted parameters in the whole processing, and is totally adaptive to the local image content.

The rest of the paper is organized as follows. Section II gives a brief review of the background algorithm – FLICM and describes our motivations for further improvements. In Section III, the proposed FLDNICM algorithm is described in details. Section IV illustrates the performance of the proposed algorithm through four experiments. Finally, Section V draws the conclusion.

II. Background and Motivations

In this section, the background algorithm – FLICM is briefly reviewed. Then, our motivations for proposing the FLDNICM clustering algorithm are introduced.

A. FLICM Algorithm

Let us consider an image $X=\{x_1, x_2, \cdots x_i, \cdots, x_n\}$, where $x_i \in \mathrm{R}^{band}$ represents a pixel in the $band-$dimensional vector space, n is the number of feature vectors (pixel number in the image), and c is the number of clusters ($2 \le c < n$). FLICM [9] introduces a fuzzy factor G_{ki} as a local similarity measure to remove noise and preserve image details.

$$G_{ki} = \sum_{\substack{j \in N_i \\ j \neq i}} \frac{1}{d_{ij}+1} (1-u_{kj})^m \| x_j - v_k \|^2 \tag{1}$$

supposing pixel x_i is the center of the local window, N_i is the set of neighborhood pixels around pixel x_i, pixel x_j ($j \in N_i$) is a neighboring pixel in N_i, d_{ij} is the spatial Euclidean distance between pixels x_i and x_j, v_k is the prototype of the center of cluster k, u_{kj} is the degree of membership value of pixel x_j belonging to the kth cluster, $\|\bullet\|$ is any norm expressing a dissimilarity measure between data points and centers, and m is the weighing exponent in each fuzzy membership. This factor m in the proposed algorithm and the above algorithms plays the same role as in FCM, which has been discussed in [33]. In this paper, we set $m=2$ for the following experiments. The objective function of FLICM is described as

$$J_m = \sum_{i=1}^{n} \sum_{k=1}^{c} \left[u_{ki}^m \| x_i - v_k \|^2 + G_{ki} \right] \tag{2}$$

where u_{ki} and v_k are:

$$\boldsymbol{v_k} = \frac{\sum_{i=1}^{n} u_{ki}^m \boldsymbol{x}_i}{\sum_{i=1}^{n} u_{ki}^m} \tag{3}$$

and

$$u_{ki} = \frac{1}{\sum_{k'=1}^{c} \left(\frac{\| x_i - v_k \|^2 + G_{ki}}{\| x_i - v_{k'} \|^2 + G_{k'i}} \right)^{1/(m-1)}} \tag{4}$$

The objective function J_m can be optimized through an iterative process, details are described in [9]. In the FLICM method, the fuzzy factor G_{ki}, which incorporates local spatial and gray level information, does not involve any tuning parameter to control the trade-off between the image noise and details, and can reflect the damping extent of neighbors with spatial distances from the central pixel. With G_{ki}, the fuzzy membership values of the non-noisy pixels, as well as the noisy pixels in the local window, will be set to similar values and this can balance the membership values of the pixels in the local window. FLICM is therefore robust to noise and outliers to some extent.

B. Motivation of Introducing the Trade-off Weighted Fuzzy Factor

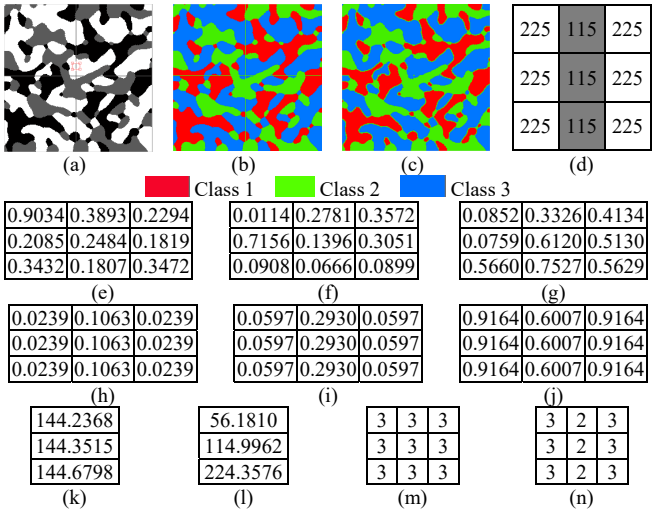

Fig. 1. Classification results of a synthetic image produced by FLICM. (a) Original image. (b) Reference image. (c) Classification map produced by FLICM. (d) A 3×3 window [marked with a red rectangle, and the central pixel locates at pixel (125,108)]. (e), (f) and (g) Initial membership degrees of the pixels belonging to the three class, respectively. (h), (i) and (j) Final membership degrees of the pixels belonging to the three classes, respectively. (k) Intial cluster centers. (l) Final cluster centers. (m) Classification results using FLICM. (n) Reference.

Spatial and gray level information are used in FLICM to guarantee noise insensitiveness and preservation of image details. FLICM can enhance the robustness and increase the accuracy of the conventional FCM to a certain extent. However, it is not adequate to reflect the damping extent of the neighbors only using the spatial distances from the central pixel. Sometimes, it is not in conformity with the discrepancy between the pixels in the neighborhood [19]. In particular, this method has some weakness in identifying the class boundary pixels and preserving details [20]. A synthetic image is used to test the preserving details performance of the FLICM method. As shown in Fig. 1(a), the synthetic image with 256×256 pixels including three classes (1, 2, and 3) with three intensity values (taken as 55, 115, and 225) is sampled from Markov Random Field (MRF) model using a Gibbs sampler. In order to test the performance of details preservation, two lines with intensity value 115 are added (see Fig. 1(b)). The parameters used in the FLICM are $c=3$, $m=2$ and $\varepsilon=1e-5$. A 3×3 window is used in the experiment. Fig. 1(c) can clearly show that the two added lines are smoothed out and many misclassified pixels locate on the regional boundaries produced by the FLICM. After 21 iterations the membership value of the central pixel converges to a value similar to those of the neighboring pixels, the central pixel is misclassified as the Class 3 to which most of its neighboring pixels belong.

The above example gives some intuitive illustrations about the limitations in identifying the class boundary pixels and preserving details while smoothing out noises. The fuzzy factor G_{ki} always imposes a significant amount of spatial constraint on the central pixel. In other words, the central pixel is influenced heavily by the neighboring pixels no matter whether it is a noise pixel or a boundary pixel. It can be dragged to the cluster center to which most of its neighboring pixels belong, thus introducing a blurring effect. This is because using single spatial distance to reflect the damping extent of the neighbors in the trade-off weighted factor in G_{ki} is not sufficient. Furthermore, according to (1), the calculation of G_{ki} is mostly based on its neighboring pixels while the central pixel's own gray information is not fully considered, which cannot accurately reflect the damping extent of the neighbors. In this context, in order to obtain more accurate classification results, it is crucial to define an accurate weighted factor for neighboring effects which is fully adaptive to the image content, and provides an accurate trade-off between insensitiveness to noise and effectiveness of preserving the details in the image. This is done in Section III-A, where we present a trade-off weighted factor based on the pixel spatial attraction model.

The enhancement of FLICM's robustness to noise and outliers is based on the incorporation of the fuzzy factor G_{ki}. However, when the images are heavily contaminated by noise, the performance of FLICM will degrade [20]. As shown in the example of Fig. 2(c), there still exist isolated pixels in the classification results provided by the FLICM. After 23 iterations, the membership value of the central pixel tries to converge to a membership value similar to that of the neighboring pixels, but it cannot reach this value and is misclassified as the Class 2.

Through the above example, we can deduce that the central pixel has been heavily influenced by its neighborhood pixels with G_{ki}, but when the gray value of the central pixel is highly different from its neighborhood pixels, the effects from its neighboring pixels described by G_{ki} are not strong enough to drag the noisy central pixel to the cluster center to which most of its neighboring pixels belong. Thus, to compensate for the deficiency of the G_{ki}, a fuzzy prior probability function is developed for incorporating the spatial contextual information like MRF. This function, which is described in detail in Section III-B, directly defines neighboring constraint on the central pixel term of the objective function, in such way that the aforementioned problem can be addressed.

C Motivation of Introducing the Fuzzy Prior Probability Function

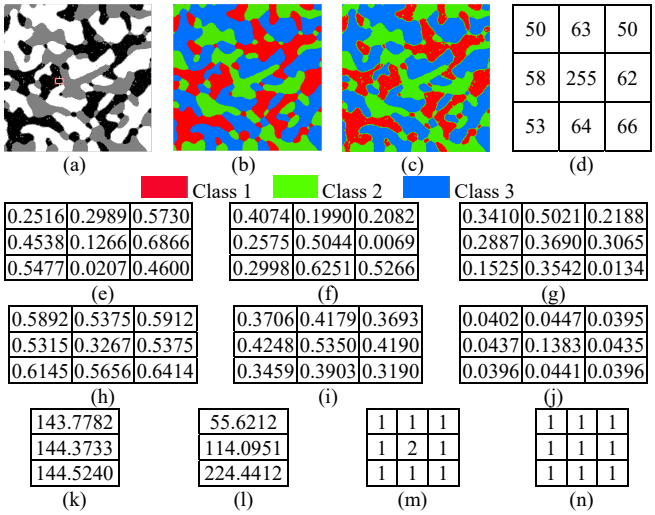

50	63	50
58	255	62
53	64	66

0.2516	0.2989	0.5730
0.4538	0.1266	0.6866
0.5477	0.0207	0.4600

0.4074	0.1990	0.2082
0.2575	0.5044	0.0069
0.2998	0.6251	0.5266

0.3410	0.5021	0.2188
0.2887	0.3690	0.3065
0.1525	0.3542	0.0134

0.5892	0.5375	0.5912
0.5315	0.3267	0.5375
0.6145	0.5656	0.6414

0.3706	0.4179	0.3693
0.4248	0.5350	0.4190
0.3459	0.3903	0.3190

0.0402	0.0447	0.0395
0.0437	0.1383	0.0435
0.0396	0.0441	0.0396

143.7782
144.3733
144.5240

55.6212
114.0951
224.4412

1	1	1
1	2	1
1	1	1

1	1	1
1	1	1
1	1	1

Fig. 2. Classification results of a synthetic image with noise produced by FLICM. (a) Original image. (b) Reference image. (c) Classification map produced by FLICM. (d) A 3×3 window [marked with a red rectangle, and the central pixel locates at pixel (94,134))]. (e), (f) and (g) Initial membership degrees of the pixels belonging to the three class, respectively. (h), (i) and (j) Final membership degrees of the pixels belonging to the three classes, respectively. (k) Initial cluster centers. (l) Final cluster centers. (m) Classification results using FLICM. (n) Reference.

III. Proposed Method

As mentioned above, motivated by the individual strengths as well as limitations of FLICM, this paper presents the FLDNICM clustering algorithm for remotely sensed imagery classification. Section III-A describes the trade-off weighted factor for introducing the spatial constraints from neighboring pixels, and Section III-B illustrates the fuzzy prior probability function for integrating spatial contextual information. The general framework of FLDNICM is shown in Section III-C.

A. A Trade-off Weighted Fuzzy Factor

Inspired by the Newton's law of universal gravitation [34], every object in the universe attracts each other. The attraction model has been also shown to be effective in characterizing the spatial relationships between pixels in an image [34], [35]. In this paper, the spatial attraction model is introduced to incorporate local spatial and gray level statistics information simultaneously. For two pixels i and r, spatial attraction between them is proportional to their fuzzy memberships u_{ki} and u_{kr} with respect to the kth cluster, and inversely proportional to the square of the spatial distance between the two pixels. Accordingly, the pixel spatial attraction $PSA_{ir}(k)$ between the two pixels with respect to the kth cluster can be defined as

$$PSA_{ir}(k) = G_r \frac{u_{ki} \times u_{kr}}{d_{ir}^2} \tag{5}$$

where d_{ir} is a spatial distance between pixels i and r. In this paper, the Euclidean distance is selected for computational simplicity. G_r is a weighted factor which controls the relative importance of the neighborhood in the local window. Let us focus on the definition of G_r.

20	180	20	160	20
20	22	B 22	20	20
100	A 22	D 20	20	20
20	20	C 20	100	20
20	20	20	20	20

(a)

20	22	B 22
100	A 22	D 20
20	20	C 20

(b)

180	20	160
22	B 22	20
A 22	D 20	20

(c)

Fig. 3. Illustration of the relative importance of different neighboring pixels. (a) A 5×5 window (extract from an image). (b) A 3×3 window [extract from (a)]. (c) A 3×3 window [extract from (a)].

As shown in Fig. 3, D is the central pixel in a 5×5 window, A and B have the same gray value, but their influences on D should be different as there is one noise pixel around A (as shown in Fig. 3(b)), whereas there are two noise pixels around B (as shown in Fig. 3(c)). In greater detail, B is influenced heavier than A by the noise, thus in order to weaken the influence of noise on the central pixel, the influence on D from B should be smaller than that from A. Here, we use the local coefficient of variation (CV) to describe the degree of influence. The CV is defined as the ratio of the standard deviation to the mean, and the local CV C_r for each pixel r is defined as

$$C_r = \frac{\sigma(x)}{\mu(x)} \tag{6}$$

where pixel r is the central pixel of the local window and pixel x represents a set of the neighboring pixels falling into the window (for example a 3×3 window) around the rth pixel, $\sigma(x)$ and $\mu(x)$ are the standard deviation and the mean of the pixel's intensity in the local window, respectively. The value of C_r can reflect gray value homogeneity degree of the local window, which explains the local distribution of pixel x. It will show high value at edge or in the area corrupted by noise, and show low value in a homogeneous window. Due to the variation of C_r in different local window, here, C_r for each pixel across the image is normalized into [0, 1]. The normalization method is formulated as

$$\xi_r = \frac{C_r - C_{\min}}{C_{\max} - C_{\min}} \tag{7}$$

where $C_{\max}$ and $C_{\min}$ are the maximum and minimum values of C_r, and respectively, ξ_r is the normalized local CV. Then G_r is defined as

$$G_r = 1 - \log_2(\sqrt{\xi_r} + 1) \tag{8}$$

where $G_r \in [0,1]$. When the local window around pixel r includes noise or edge pixels, the value of G_r is small and close to 0, the effect from pixel r will be weaken and, according to (5), the value of $PSA_{ir}(k)$ will become small; thus the

influence from noise or outliers will be suppressed, and vice versa. In addition, G_r also helps to exploit more local context information because the local CV of each pixel is computed in its local window.

As described above, it is crucial to provide an accurate trade-off weighted factor for neighboring effect in $G_{ki}^{'}$. While the pixel spatial attraction model, which changes flexibly according to their spatial distances from the central pixel and fuzzy membership's differences simultaneously, can exactly describe the relationships between pixels. Based on the spatial attraction model, we introduce a trade-off weighted fuzzy factor $w_{ir}(k)$ incorporating both the local spatial and fuzzy membership relationships. It is defined as

$$w_{ir}(k) = \lambda_i \frac{PSA_{ir}(k)}{\sum_{r\in N_i, r\neq i} PSA_{ir}(k)} \tag{9}$$

where λ_i represents the gray value homogeneity degree within the local window. It is used to model the complexity of the portion of image located within the local window, and is defined as

$$\lambda_i = \sum_{r\in N_i} \xi_r \tag{10}$$

where ξ_r is the normalized local CV at the considered local window (see Fig. 4(c)). When the neighboring pixels and the central pixel are all located in a homogeneous region, the value of λ_i will be small and the complexity degree within the local window will be low, and vice versa. Here, $PSA_{ir}(k)$ is the pixel spatial attraction between the central pixel i and its neighboring pixel r with respect to the kth cluster. For computational simplicity, the size of N_i is set as 3×3. (see Fig. 4(a)). The rationale is as follows:

1) The pixel spatial attractions are active only within the 3×3 window and are neglected outside.

2) The pixel spatial attractions is active only between the same class sub-pixels (denoted by the fuzzy memberships) contained in the central pixel and its neighbor.

$N_{i,1}$	$N_{i,2}$	$N_{i,3}$
$N_{i,4}$	i	$N_{i,5}$
$N_{i,6}$	$N_{i,7}$	$N_{i,8}$

(a)

$\sqrt{2}$	1	$\sqrt{2}$
1	i	1
$\sqrt{2}$	1	$\sqrt{2}$

(b)

ξ_1	ξ_2	ξ_3
ξ_4	ξ_5	ξ_6
ξ_7	ξ_8	ξ_9

(c)

Fig. 4. Trade-off weighted fuzzy factor at the neighbor of pixel i at 3×3 window: (a) Neighbor of pixel i. (b) Distances between pixel i and its neighbor. (c) Normalized local coefficient of variation at a 3×3 window.

It is worth noting that the proposed trade-off weighted fuzzy factor $w_{ir}(k)$ does not involve any experimentally adjusted parameter in the whole processing, the information needed to compute this factor is totally based on the central and its neighborhood pixels, thus, it is totally adaptive to the local image content. The main characteristics of the resulting technique are as follows:

1) It can accurately describe the relationships between the central and neighboring pixels using the local spatial and gray level statistics information simultaneously;

2) The central pixel is influenced by its neighbors and its own features simultaneously, which is important for retaining edges of regions and small patches when removing noise;

3) The degrees of fuzzy memberships of pixels are used to describe the fuzzy factor, which is finer than using differences of intensity, because different weighted factors are exploited for different classes. This is very useful to correctly classify the class boundary or edge pixels, because these pixels have similar distances to their adjacent cluster centers. If the differences of intensity is used, the pixel with high gray difference will influence the central pixel heavier, which often results in misclassification. On the contrary, fuzzy memberships can accurately describe the memberships of each pixel to each class;

4) With λ_i, the spatial constrains from $G_{ki}^{'}$ can be adaptively adjusted with the complexity of the portion of image located within the local window

B. A Fuzzy Prior Probability Function

As described in Section II-C, when the gray value of the central pixel is highly different from its neighborhood pixels' gray values, $G_{ki}^{'}$ as well as G_{ki} may have deficiencies to properly represent the situation. To compensate for the deficiency, it is very important to further enhance the FLDNICM's robustness to noise and outliers. In this section, firstly, the local prior probability based on MRF model is briefly introduced. Then, a fuzzy prior probability function is provided for incorporating spatial contextual information to enhance the FLDNICM's robustness performance.

The MRF is a probabilistic model which extracts spatial contextual information through the dependence among neighboring pixels [36]. It is widely used to improve the classification accuracy by incorporating spatial contextual information [37]-[39].

According to the Harmmersley-Clifford theorem and the Gibbs theorem [40], the local prior probability $P_{ki}^{'}$ can be represented as

$$P_{ki}^{'} = \frac{\exp(-\mathrm{E}_i(k))}{\sum_{k'=1}^{c}\exp(-\mathrm{E}_i(k'))} \tag{11}$$

where $\mathrm{E}_i(k)$ is the energy function of pixel x_i with respect to the kth cluster, which is defined as

$$\mathrm{E}_i(k) = \beta\sum_{j\in N_i} I(k(x_i), k(x_j)) \tag{12}$$

$$I(k(x_i), k(x_j)) = \begin{cases} -1 & k(x_i) = k(x_j) \\ 0 & k(x_i) \neq k(x_j) \end{cases} \tag{13}$$

where N_i denotes the neighbors of pixel x_i, $i \notin N_i$, $k(x_i)$ denotes the class label of pixel x_i, $k(x_j)$ is the neighboring class label of pixel x_i, $j \in N_i$. Equation (13) is the Potts model

in MRF, and is used to describe the class label prior probability, β is a penalty coefficient which is used to control the strength between pixel x_i and its neighboring pixels. The local prior probability based on MRF directly characterizes the spatial context and serves as an operator to exploit the information provided by the neighboring pixels, and it is often used to mitigate noise effects [36].

However, the prior probability function in Equation (12) is only computed by comparing the labels of the neighboring pixels regardless of both the local image statistics and whether the neighboring pixel is a boundary pixel or not. Furthermore, the neighboring pixels have the equal influences on the central pixel x_i. As a result, the classification accuracy is improved in homogeneous areas, while errors frequently occur on boundary areas, thus losing significant detailed features. Besides, the choice of the penalty coefficient β is difficult and time-consuming. Thus, the traditional MRF model has significant limitations in real applications.

Motivated by the above-mentioned discussion, a fuzzy prior probability function P_{ki} is proposed defined as

$$P_{ki}=\overline{\xi_i}\frac{\exp[-\sum_{r\in N_i,r\neq i}(1-|u_{ki}-u_{kr}|)]}{\sum_{k'=1}^{c}\exp[-\sum_{r\in N_i,r\neq i}(1-|u_{k'i}-u_{k'r}|)]} \tag{14}$$

where $|u_{ki}-u_{kr}|$ stands for the absolute difference between memberships u_{ki} and u_{kr}. Here, a 3×3 window is used consistently with the definition of $w_{ir}(k)$. $\overline{\xi_i}$ is the average gray value homogeneity degree of the local window, and is used to denote penalty coefficient to control the strength between pixel x_i and its neighboring pixel. It is defined as

$$\overline{\xi_i}=\frac{\sum_{r\in N_i}\xi_r}{n_i} \tag{15}$$

where n_i is the number of pixels located in the local window (see Fig. 4(c)).

As shown in Equation (14), there are no experimentally adjusted parameters in the proposed probability prior function. It utilizes the fuzzy memberships to model the effects on the central pixel from neighboring pixels. The neighboring pixels have different influences on the central pixel, thus it can preserve local details information: 1) When the central pixel is heavily corrupted by noise, while the other pixels in its local window are homogeneous, the P_{ki} should be chosen as high as possible so that the clustering result of the central pixel is greatly influenced by its neighbors. As we can see from Equation (14), in this case, the value of P_{ki} is relatively high, in such way that the central pixel will be assigned with high membership to the class to which its most neighboring pixels belong. 2) When the central pixel is not corrupted by noise, while the other pixels in its local window are homogeneous, the P_{ki} should be chosen as small as possible so that the clustering result of the central pixel depends mainly on its own intensity information. As can see from Equation (14), in this case the value of P_{ki} is relatively small.

C. General Framework of FLDNICM Algorithm

Based on the trade-off weighted fuzzy factor $w_{ir}(k)$ and the fuzzy prior probability function P_{ki}, FLDNICM is proposed for unsupervised remotely sensed imagery classification. It incorporates flexible and accurate local spatial and spectral information into the objective function of conventional FCM to enhance the smoothness towards piecewise-homogeneous classification and reduce the edge blurring effect simultaneously, the objective function of FLDNICM is described as:

$$J_m^{'}=\sum_{i=1}^{n}\sum_{k=1}^{c}\left[u_{ki}^m(1-P_{ki})\|x_i-v_k\|^2+G_{ki}^{'}\right] \tag{16}$$

and the new fuzzy factor $G_{ki}^{'}$ in Equation (16) is defined as

$$G_{ki}^{'}=\sum_{r\in N_i,r\neq i}w_{ir}(k)(1-u_{kr})^m\|x_r-v_k\|^2 \tag{17}$$

where x_i is the gray value of the *i*th pixel, N_i is the set of neighborhood pixels in the window around the pixel x_i, the shape of local window used in our experiments is square (however other shapes such as diamond or circle can also be adopted in our algorithm), pixel x_r is the neighboring pixel that falls into N_i, v_k denotes prototype value of the *k*th cluster, u_{ki} and u_{kr} represent the degree of fuzzy membership of x_i and x_r belonging to the *k*th cluster, respectively. $w_{ir}(k)$ and P_{ki}, which will be provided by (9) and (14), are the trade-off weighted factor between x_i and x_r in the local window and the fuzzy prior probability function with respect to the *k*th cluster, respectively. The two necessary conditions of $J_m^{'}$ to be at its local minimal extreme with respect to u_{ki} and v_k are obtained as follows:

$$\boldsymbol{v}_k=\frac{\sum_{i=1}^{n}u_{ki}^m(1-P_{ki})\boldsymbol{x}_i}{\sum_{i=1}^{n}u_{ki}^m(1-P_{ki})} \tag{18}$$

$$u_{ki}=\frac{1}{\sum_{k'=1}^{c}\left(\frac{\|x_i-v_k\|^2(1-P_{ki})^2+G_{ki}^{'}}{\|x_i-v_{k'}\|^2(1-P_{k'i})^2+G_{k'i}^{'}}\right)^{1/(m-1)}} \tag{19}$$

The flowchart of the proposed method is shown in Fig. 5. The implementation includes the following five steps.

Step 1 *(Initialization):* Changing the dimension of input data to *n*×*band* dimension, set the cluster number c, the weighted exponent m, the window size N_i, the termination criterion ε and the loop counter $b=0$. The standard FCM is implemented to obtain the final fuzzy memberships matrix $U=\{u_{ki}\}_{c\times n}$ as the initial memberships matrix of FLDNICM.

Step 2 *(Calculating* $G_{ki}^{'}$ *and* P_{ki}*):* The new fuzzy factor $G_{ki}^{'}$ and the prior probability function P_{ki} are calculated according to (17) and (14), respectively.

Step 3 *(Calculating the Cluster Centers and Membership Values):* Based on the $G_{ki}^{'}$ and P_{ki} values obtained in Step 2, the cluster centers and the membership values are calculated by using (18) and (19), respectively.

Step 4 *(Termination):* The iteration will stop when the termination criterion $\max_{k\in[1,c]}\{\|v_k^b - v_k^{(b+1)}\|\} < \varepsilon$ is met; otherwise, $b = b+1$, go back to Step 2 and repeat.

Step 5 *(Assigning the Final Class to Each Pixel):* When the algorithm converges, the final fuzzy matrix $U = \{u_{ki}\}_{c\times n}$ is produced, and the crisp partition is obtained by assigning each pixel i to the class c having the greatest membership, i.e.

$$C_i = \arg_k\{\max(u_{ki})\},\ k = 1,2,3,\cdots,c \qquad (20)$$

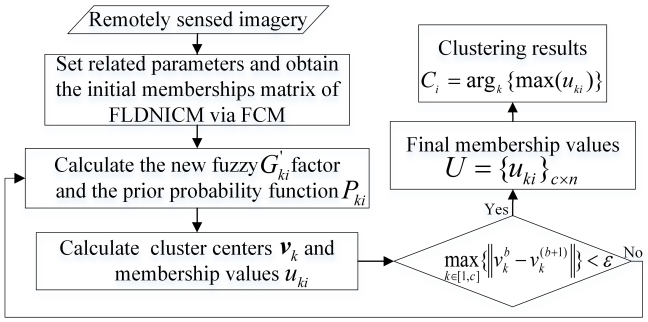

Fig. 5. Flowchart of the proposed FLDNICM clustering algorithm.

As one can see from (16), the objective function of the proposed FLNDICM contains two constraint components. Left one puts constraints directly on the central pixel to be close to the cluster centers with a given prior probability function. The other imposes spatial continuity by introducing a trade-off weighted fuzzy factor. These two terms are determined automatically and adaptively to the local image content. These two kinds of spatial contextual information and spatial constraints make FLDNICM produces homogeneous clustering results and reduces the edge blurring artifacts simultaneously. Three basic cases are used to describe the robustness to noise and details preservation ability of the FLDNICM algorithm.

Case 1: The central pixel is not noisy and some of its neighboring pixels are contaminated by noise. An example is shown in Fig. 6. A 3×3 window for the pixel marked in Fig. 6(a) is shown as Fig. 6(b). FLDNICM converges after 25 iterations. As shown in Fig 6(b), the gray level values of noisy pixels are 0 and 255, which are far different from the central pixel having a value of 117. The proposed trade-off weighted fuzzy factor and prior probability function balance their membership values and suppress the influences from noise of the neighbors. Taking the central pixel as an example, Table I quantitatively reports how the spatial constraints in the FLDNICM method influence the central pixel. In order to suppress the influences of the outlier, the weights associated with the noise pixels should be smaller than those of these pixels without noise. Fig. 6(j) just shows that the weights on the noise pixels are relatively smaller than those pixels without noise with respect to Class 2, the more the noise pixel is corrupted, the smaller the weight value is. And Fig. 6(i) and (k) show weights on the noise pixels are relatively higher than those pixels without noise with respect to Class 1 and 3, respectively. Then, the weighting added the spatial constraint is increased to suppress the influence of the outliers. The prior probability of P_{2i} is also the highest one and the value of $G_{2i}^{'}$ becomes the smallest one with respect to three classes, as a result, the probability of the central pixel is classified into the Class 2 is increased and then classified as Class 2. Thus, the proposed method becomes more robust to outliers.

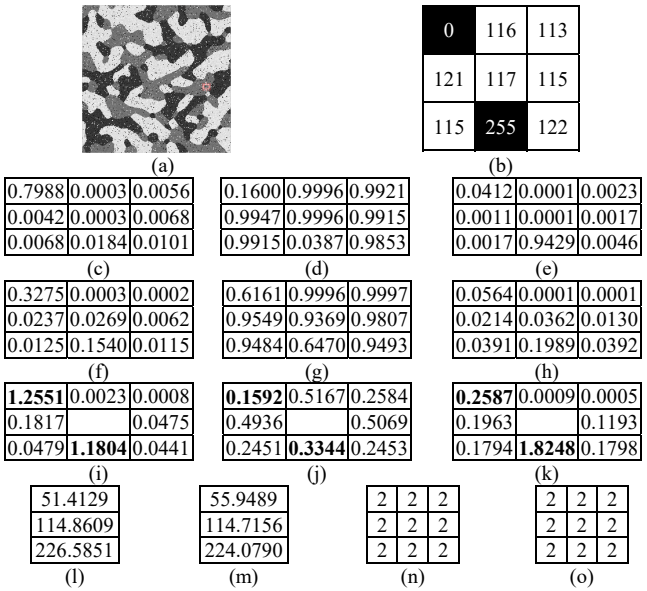

Fig. 6. Classification results of a synthetic image with noise using FLDNICM (Case 1). (a) Original image. (b) A 3×3 window [marked with a rectangle in the original image, and the central pixel locates at pixel (214, 142)]. (c), (d) and (e) Initial membership degrees of the pixels belonging to the three class, respectively. (f), (g) and (h) Final membership degrees of the pixels belonging to the three classes after 25 iterations, respectively. (i), (j) and (k) Weights of $w_{ir}(k)$ with respect to the three classes respectively. (l) Intial cluster centers. (m) Final cluster centers. (n) Classification results using FLDNICM. (o) Reference.

TABLE I

QUANTITATIVE ANALYSIS OF THE INFLUENCE OF THE SPATIAL CONSTRAINTS OF FLDNICM ON THE CENTRAL PIXEL IN CASE 1

	Class 1	Class 2	Class 3
$\|\| x_i - v_k \|\|^2$	3727.2368	**5.2185**	11465.9122
P_{ki}	0.1084	**0.1478**	0.0888
$\|\| x_i - v_k \|\|^2 (1-P_{ji})^2$	2963.1000	3.7902	9519.6838
$G_{ki}^{'}$	36507.4089	**1129.0186**	19783.2571
$\|\| x_i - v_k \|\|^2 (1-P_{ki})^2 + G_{ki}^{'}$	39470.5089	**1132.8088**	29302.9409

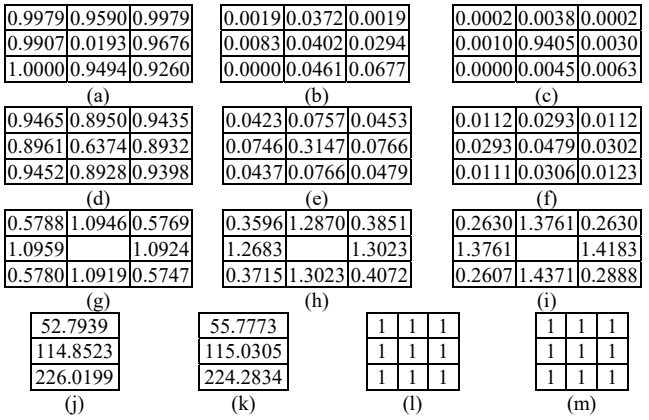

Fig. 7. Classification of a synthetic image with noise at a 3×3 window by FLDNICM (Case 2). (a), (b) and (c) Initial membership degrees of the pixels belonging to the three class, respectively. (d), (e) and (f) Final membership degrees of the pixels belonging to the three classes, respectively. (g), (h) and (i) Weights of $w_{ir}(k)$ with respect to the three classes, respectively. (j) Intial cluster centers. (k) Final cluster centers. (l) Classification results using FLDNICM. (m) Reference.

TABLE II

QUANTITATIVE ANALYSIS OF THE INFLUENCE OF THE SPATIAL CONSTRAINTS OF FLDNICM ON THE CENTRAL PIXEL IN CASE 2

	Class 1	Class 2	Class 3
$\| x_i - v_k \|^2$	39689.6842	19591.4609	**943.5095**
P_{ki}	**0.4318**	0.3472	0.0564
$\| x_i - v_k \|^2 (1-P_{ji})^2$	12813.2589	8348.0365	840.0202
$G_{ki}^{'}$	**2.3666**	17596.9819	169566.7196
$\| x_i - v_k \|^2 (1-P_{ki})^2 + G_{ki}^{'}$	**12815.6256**	25945.0184	170406.7398

Case 2: The central pixel is noisy and the pixels within its local window are not contaminated and homogeneous. Just shown as in Fig. 2(a) and (b), the gray value of the central pixel is 255, which is a salt and pepper noise and far different from those of the neighbors. The FLICM method had misclassified the central pixel as Class 2. While the FLDNICM method converged after 27 iterations and pushes the membership value of the central pixel to the same as that for the non-noisy neighbors (see Fig. 7). To quantitatively describe how the spatial constraints influence the central pixel, taking the central pixel as an example, as can been seen from Table II, the central pixel should be classified as the Class 3 according to the values of $\| x_i - v_k \|^2$, while its neighboring pixels all belong to Class 1, we can see the value of prior probability of P_{1i} is the highest one and the value of $G_{1i}^{'}$ becomes the smallest one with respect to three classes, as a result, pushing the class of central pixel to the same as most neighbors belonging to, and, hence, the FLDNICM becomes more robust to outliers.

Case 3: In Cases 1 and 2, pixels in the given local window are homogeneous. However, there are also pixels located on the object (or class) boundaries, like in Fig. 1(a) and (d). In this example, the FLICM method misclassified the line with gray value 115 as Class 3, while the FLDNICM method converged after 26 iterations preserving the details (see Fig. 8). Taking the central pixel as an example, Table III shows that the central pixel should be classified as the Class 2 according to the values of $\| x_i - v_k \|^2$, while most of its neighboring pixels belong to Class 1. The FLDNICM properly recognizes this situation, and thus the central pixel is not heavily influenced by its neighboring pixels. The prior probability of P_{ki} is relatively small, because the P_{ki} is defined based on the fuzzy memberships of both the central pixel and the neighboring pixels, and the neighboring pixels have different influences on the central pixel. Accordingly, due to the fuzzy modeling, it can preserve more local details information. Moreover, as $w_{ir}(k)$ utilizes the pixel spatial attraction model to describe the trade-off weighted fuzzy factor, different weighted factors are derived with respect to different classes according to their memberships and distances from the center. Thus the trade-off not only incorporates the neighborhood pixels' spatial and gray level information, but also the central pixel's own gray level information. As shown in the classification result of FLDNICM, the central pixel is correctly assigned to Class 2, confirming that the proposed method can keep a balance between the insensitiveness to noise and the effectiveness in preserving details.

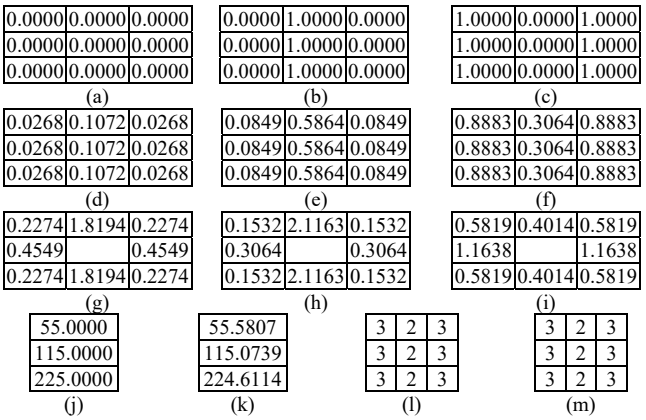

Fig. 8. Classification of a synthetic image at a 3×3 window by FLDNICM (Case 3). (a), (b) and (c) Initial membership degrees of the pixels belonging to the three class, respectively. (d), (e) and (f) Final membership degrees of the pixels belonging to the three classes, respectively. (g), (h) and (i) Weights of $w_{ir}(k)$ with respect to the three classes respectively. (j) Intial cluster centers. (k) Final cluster centers. (l) Classification results using FLDNICM. (m) Reference.

TABLE III

QUANTITATIVE ANALYSIS OF THE INFLUENCE OF THE SPATIAL CONSTRAINTS OF FLDNICM ON THE CENTRAL PIXEL IN CASE 3

	Class 1	Class 2	Class 3
$\| x_i - v_k \|^2$	3530.6532	0.0055	12014.6590
P_{ki}	0.0086	0.1082	0.1752
$\| x_i - v_k \|^2 (1-P_{ji})^2$	3469.8670	0.0043	8173.0387
$G_{ki}^{'}$	25553.9144	5308.4213	1986.3483
$\| x_i - v_k \|^2 (1-P_{ki})^2 + G_{ki}^{'}$	29023.7814	5308.4257	10159.3870

A synthetic image with mixed noise is used to further illustrate the robustness and details preservation properties of the proposed FLDNICM method compared with the FLICM

method. Fig. 9(a)-(c) show the corrupted image and the classification results provided by the FLDNICM and the FLICM. The synthetic image was generated with mixed noises including 'Gaussian' noise (mean = 0, variance = 0.01), 'Salt and Pepper' noise (density = 0.05) and 'Speckle noise' (mean = 0, variance = 0.04). As shown in Fig. 9, the FLICM produces a map with salt and pepper noise and misclassified boundary pixels, while in the classification result of the FLDNICM most of the isolated pixels are removed and edge details are satisfactorily classified. Thus, FLDNICM outperforms FLICM in terms of both robustness to noise and identification of region boundaries. To evaluate the performances quantitatively, the Producer's accuracy (PA), Overall Accuracy (OA) and Kappa coefficient (KC) [41] are listed in Table IV. As one can see from the table, FLDNICM yields greater classification accuracies than FLICM.

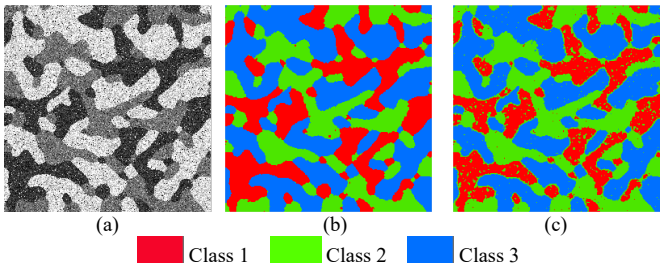

Fig. 9. Classification results for a synthetic image with composite noises using FLDNICM and FLICM. (a) Corrupted image. (b) and (c) Classification maps produced by FLDNICM and FLICM, respectively.

TABLE IV
COMPARISON OF PA, OA AND KAPPA COEFFICIENT OBTAINING BY FLDNICM AND FLICM (SYNTHETIC IMAGE WITH COMPOSITE NOISES)

Class	Number of Testing samples	FLDNICM	FLICM
Class 1	19145	97.67%	81.49%
Class 2	18360	97.84%	97.85%
Class 3	28031	99.11%	96.21%
OA		98.33%	92.37%
KC		0.9745	0.8836

Moreover, to quantitatively evaluate the cluster validity of the FLICM and FLDNICM, other literature indices are given Table V (i.e., Partition Coefficient (PC) [42], Partition Entropy (PE) [43], Modification of the Partition Entropy (MPC) [44], Fukuyama and Sugeno (FS) [45], Xie-Beni (XB) [46], Kwon (K) [47], Tang (T) [48] and Partition Coefficient and Exponential Separation (PCAES) [49] indices). As one can see from the table, all indices show that FLDNICM outperforms FLICM in terms of cluster validity.

TABLE V

COMPARISON OF CLUSTER VALIDITY VALUES FOR FLDNICM AND FLICM (SYNTHETIC IMAGE WITH COMPOSITE NOISES)

Algorithm	V_{PC}	V_{PE}	V_{MPC}	V_{FS}	V_{XB}	V_K	V_T	V_{PCAES}
FLDNICM	0.8967	0.2919	0.8451	-2.6969E+08	0.2930	2.2311E+04	2.2310E+04	2.5659
FLICM	0.7969	0.5437	0.6954	-2.5965E+08	0.3466	2.2717E+04	2.2717E+04	3.0153

The above analyses gives some intuitive illustrations about the robustness and details preservation of our algorithm. The enhancement of its robustness to noise and outliers is based on the incorporation of the $G_{ki}^{'}$ with fuzzy local spatial and gray level constraints and of P_{ki} with spatial contextual information constraints. The control of the balance between the image noise and the image details is automatically achieved by the definition of the trade-off weighted fuzzy factor and the prior probability function. The main characteristics of FLDNICM are summarized as follow:

1) It is free of any parameter selection in the whole processing, and the trade-off weighted fuzzy factor and prior probability function are totally adaptive to the local image content;

2) The relationships between the central pixel and its neighbor pixels are accurately described by the pixel spatial attraction model, which provides fine trade-off weighted fuzzy factors with respect to different classes. Here, the central pixel is simultaneously influenced by both its neighboring pixels and its own features. This is important for retaining edges of regions and small patches when removing noise;

3) By introducing the trade-off weighted fuzzy factor and prior probability function, the proposed algorithm becomes less sensitive to outliers in a relative strong noisy environment compared to other FCM with spatial variants and can reduce the edge blurring artifacts when removing isolated pixels.

IV. EXPERIMENTAL STUDY AND ANALYSIS

To assess the effectiveness of FLDNICM, its performances are analyzed and compared with standard FCM, FCM_S1, FLICM and AMASFC [25] through four experiments. Each algorithm is run ten times and the average classification accuracy, as well as the optimal classification results, are derived. All algorithms are implemented with Matlab 2013b. The PA, OA and KC are used to quantitatively evaluate the classification performance. The randomly initialized fuzzy partition matrix is used as the initial membership's matrix of FCM. To make it fair, the final fuzzy memberships matrix obtained from the FCM is taken as the initial membership's matrix of other compared methods, respectively.

A. Parameter Settings

In fact, FCM_S1 has a crucial parameter α required to be adjusted for clustering, its selection will obviously influence the clustering result. In this section, we focus on discussion on α selection for the next experiments. We repeat tests using FCM_S1 with different α by step 0.05 in the interval [0.2, 8] in experiments 1, 2 and 3. Fig. 10(a)-(c) shows the OA curves obtained with different α for FCM_S1. Seen from Fig. 10, in each experiment, the OA ascended with the increasing of α, and reached the peak value, then declined. FCM_S1 obtains the highest OA at α =4.32, 3.89 and 4.64 in experiments 1, 2 and 3, respectively. For the experiment 4, to compare fairly with AMASFC, α is set as 2.1 which is same as the value in experiment 3 in [25]. Referring from [25], for the four experiments, sizes of population in AMASFC are set as 30, 20, 15 and 50, respectively. The number of maximum generations is 100. The parameter δ in GLS is 1.

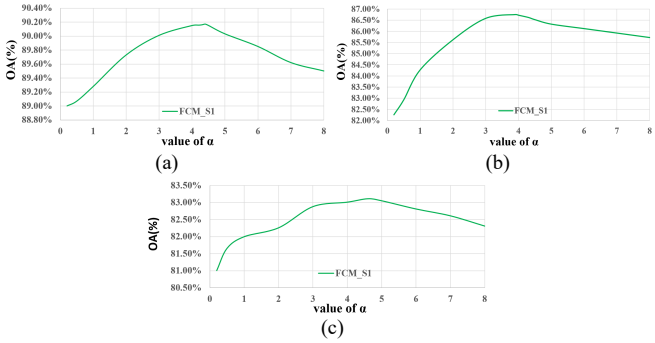

Fig. 10(a)-(c) shows the OA obtained with different α for FCM_S1 algorithm tested in Experiments 1, 2, 3, respectively.

B. Experiment 1: TM Image of Xuzhou

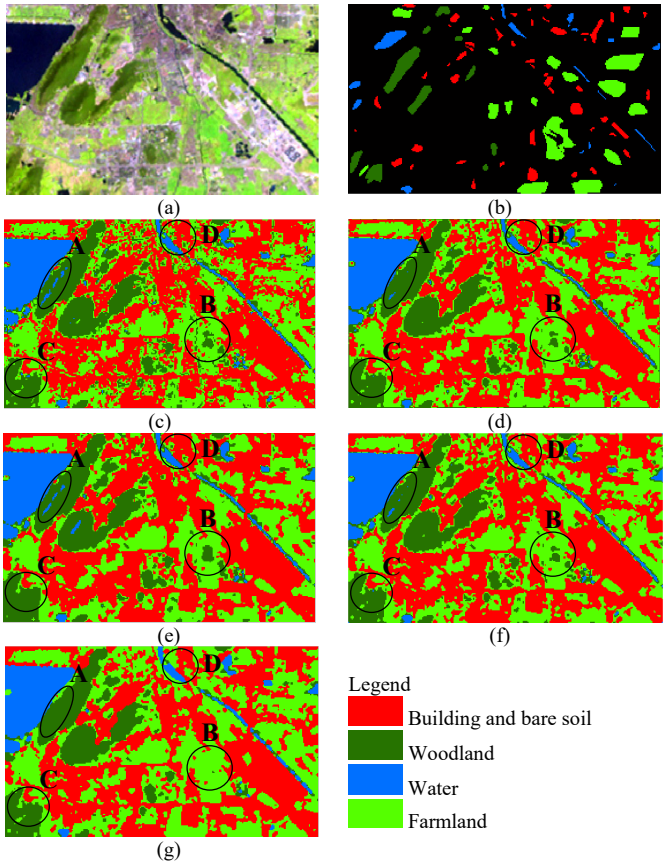

Fig. 11. Dataset and classification results in Experiment 1. (a) TM image of Xuzhou [RGB (5, 4, 3)]. (b) Reference image, (c)-(g) Classification maps produced by FCM, FCM_S1, FLICM, AMASFC and FLDNICM respectively.

In this experiment, a portion of 272×165 pixels of a multispectral Landsat Thematic Mapper (TM) image is used, which was acquired on September 14, 2000 (Fig. 11(a)) with a resolution of 30m×30m. The studied area is located in Xuzhou City, China. Bands 1, 2, 3, 4, 5 and 7 were used for image classification. The study area contains four classes: building and bare soil, woodland, water and farmland (Fig. 11(b)). The testing samples in the reference image were obtained by referring to the TM image and land use map in September 2015. Specifically, a 1: 2000 land use map collected from Xuzhou Municipal Bureau of Land and Resources, which was produced on August 2, 2000, was used. Based on the land use map, TM image and fieldwork, some reliable test sample points were selected to generate the reference map. The parameters values in the five considered algorithms are $c=4$, $\varepsilon=1e-5$ and α=4.32 for FCM_S1.

Fig. 11(c)-(g) illustrates the classification results derived by the FCM, FCM_S1, FLICM, AMASFC and FLDNICM algorithms which converged after 30, 90, 81, 79 and 72 iterations, respectively. As shown in Fig. 11(c), due to mixed pixels in the TM image and to spectral variation, FCM produces a map with salt and pepper noise and shows the weakest performance amongst the five algorithms. When the local spatial information and gray level information are incorporated into the objective function, FCM_S1, FLICM, AMASFC and FLDNICM produce more homogeneous maps. In Fig. 11(d) and Fig. 11(e), most of the isolated pixels are removed by FCM_S1 and FLICM, but some isolated pixels remain. As shown in Fig. 11(e)-(g), FLICM, AMASFC and FLDNICM are more effective in removing isolated pixels. FLICM and AMASFC remove almost all the isolated pixels and achieves satisfactory results, whereas some image details are lost. In FLDNICM results, most of the isolated pixels are removed and image details are satisfactorily preserved. For example, in marked area A, many woodland pixels are misclassified as water pixels by FCM, FCM_S1, FLICM and AMASFC, whereas FLDNICM produces more accurate result. In marked area B, many farmland pixels are misclassified into woodland pixels by FLICM and AMASFC, whereas most of the pixels are correctly classified into farmland by FLDNICM. The advantage of FLDNICM can be similarly illustrated by comparison for marked areas C and D. In area C, FLICM and AMASFC obtain more homogeneous classification results than FLDNICM. However, area C covers woodland with some farmland pixels (i.e., heterogeneous). Compared with FLICM and AMASFC, FLDNICM correctly contains more details. This experiment also illustrates that FLDNICM has advantages in classification of both homogeneous and heterogeneous landscapes.

TABLE VI

COMPARISON OF PA, OA AND KC OF FIVE CLASSIFICATION METHODS (EXPERIMENT 1)

Class	Number of Testing samples	FCM	FCM_S1	FLICM	AMASFC	FLDNICM
Building and bare soil	1275	93.02%	93.49%	96.24%	94.51%	91.06%
Woodland	1186	93.76%	98.88%	92.50%	97.98%	99.92%
Water	627	98.72%	95.73%	98.41%	97.77%	96.81%
Farmland	2647	80.36%	83.43%	83.26%	85.30%	91.39%
OA		87.95%	90.17%	89.71%	91.33%	93.67%
KC		0.8285	0.8595	0.8534	0.8756	0.9097

The quantitative results are reported in Table VI. As we can see, FCM_S1, FLICM, AMASFC and FLDNICM yield higher classification accuracies than FCM. Amongst all, FLDNICM achieves the highest OA. Taking the OA as an example, FLDNICM achieves a value of 93.67%, with gain of 5.72%, 3.50%, 3.96% and 2.34% over FCM, FCM_S1, FLICM, and AMASFC, respectively.

FLDNICM achieves the best performance both visually and quantitatively for most classes. The reasons may be that FCM does not use any spatial information in the objective function, thus resulting in poor results on isolated pixels. For the other four FCM spatial variants, in FCM_S1 the selection of parameter α value is difficult and improper α values pose poor constraints on the spatial information in the objective function, thus resulting in inaccurate predictions. Moreover, a fixed α value also blurs the image features like sharp edges while smoothing out noise. In FLICM, the classification of the central pixel is greatly influenced by its neighboring pixels but the central pixel's own feature is not fully considered. Thus, it may produce over-smoothed results for important structures and small patches. In AMASFC, although the α can be adaptively determined, the central pixel's own feature is not also fully considered, thus, over-smoothed results often exist in the result map. On the contrary, in FLDNICM by introducing the trade-off weighted fuzzy factor and prior probability function, the weighted factor can be accurately estimated and it is not only influenced by its neighboring pixels but also by the central pixel. This provides a more accurate trade-off between the central pixel and its neighboring pixels. Hence, the FLDNICM can reduce the edge blurring artifacts and preserve small patches when removing isolated pixels.

C. Experiment 2: ZY-3 Image of Xuzhou

In the experiment, a portion of 400×400 pixels of a multispectral ZY-3 image is used, which was acquired on August 11, 2012 (Fig. 12(a)) with a resolution of 6m×6m. The studied area is located in Xuzhou City, China. The four multispectral bands of the ZY-3 image were used for image classification. The reference image contains building and bare soil, greenhouse, water and vegetation (Fig. 12(b)). Based on the panchromatic imagery with 2-m resolution, the multispectral imagery and the fieldwork, the testing samples were extracted (see Fig. 12(b)) in September 2015. The parameters used in this experiment are $c=4$, $\varepsilon=1e-5$ and α=3.89 for FCM_S1.

Fig. 12(c)-(g) shows the classification results provided by the FCM, FCM_S1, FLICM, AMASFC and FLDNICM algorithms which converged after 32, 66, 89, 80 and 87 iterations, respectively. A large amount of salt and pepper noise is present in the FCM result due to the missing use of spatial information. FCM_S1, FLICM and AMASFC enhance FCM results, but show weaker performance than FLDNICM. This can be illustrated by referring to marked areas A-D. In marked area A and B, many building and bare soil pixels are misclassified as water pixels by FCM, FCM_S1, AMASFC, and many building pixels are misclassified as greenhouse pixels by FLICM. Similar results were obtained in the marked C and D areas, where FLICM achieves more homogeneous classification result than FCM, FCM_S1 and AMASFC, but details are removed while smoothing noise pixels. On the contrary, FLDNICM can correctly preserve more details and reduce the edge blurring artifacts when removing isolated pixels. This experiment also illustrates that FLDNICM has advantages in classification of both homogeneous and heterogeneous landscapes.

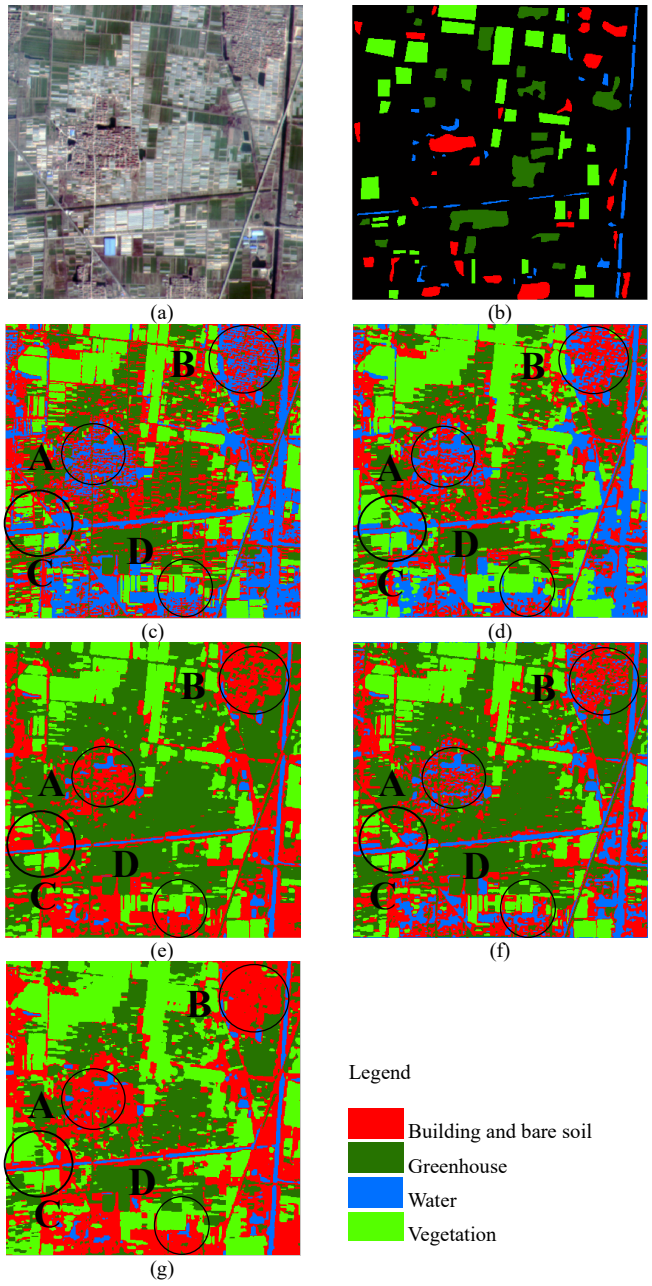

Fig. 12. Dataset and classification results in Experiment 2. (a) ZY-3 image of Xuzhou [RGB (3, 2, 1)]. (b) Reference image. (c)-(g) Classification maps produced by FCM, FCM_S1, FLICM, AMASFC and FLDNICM, respectively.

TABLE VII

COMPARISON OF PA, OA AND KC OF FIVE CLASSIFICATION METHODS (EXPERIMENT 2)

Class	Number of Testing samples	FCM	FCM_S1	FLICM	AMASFC	FLDNICM
Building and bare soil	6289	43.01%	49.85%	71.44%	59.29%	90.32%
Greenhouse	8029	90.66%	93.72%	99.93%	99.79%	98.18%
Water	2697	99.89%	99.94%	98.29%	99.85%	99.07%
Vegetation	12048	93.19%	98.46%	93.84%	93.91%	98.74%
OA		82.26%	86.77%	91.09%	88.30%	96.79%
KC		0.7525	0.8133	0.8722	0.8341	0.9539

Table VII shows that FLDNICM again produces the highest OA and KC values. The accuracy gains of FLDNICM over FCM, FCM_S1, FLICM and AMASFC are 14.53%, 10.02%, 5.70% and 8.49%, respectively.

D.Experiment 3: QuickBird Image of Xuzhou

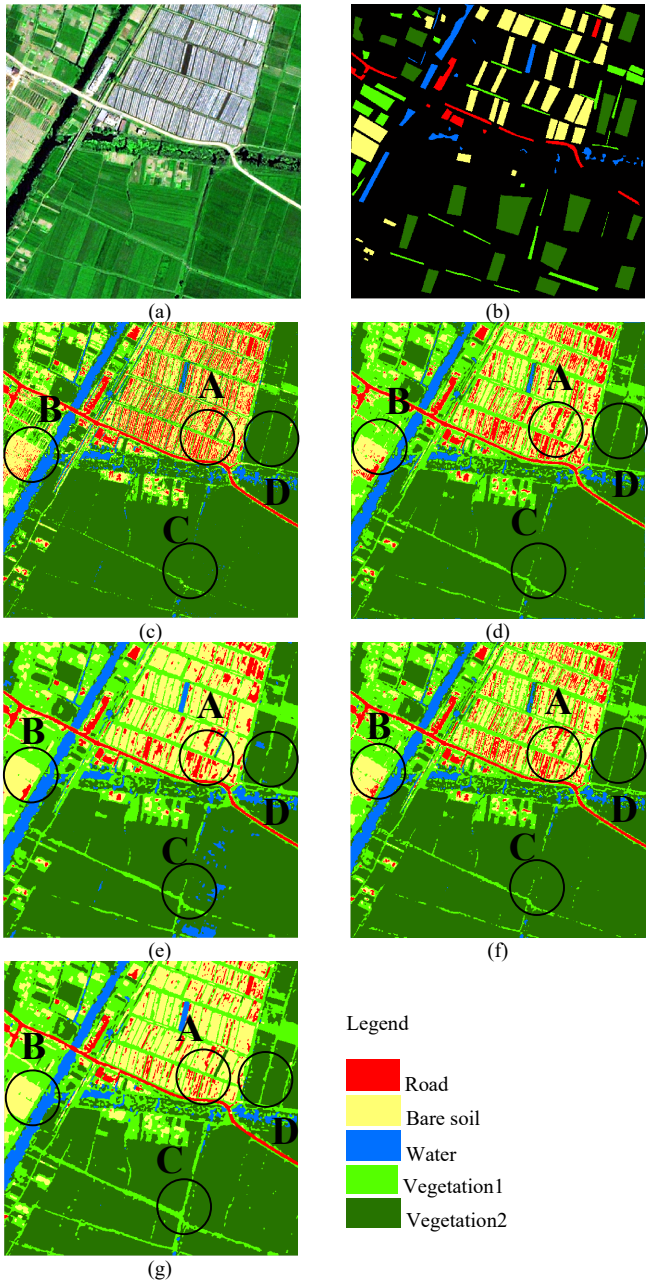

Fig. 13. Dataset and classification results in Experiment 3. (a) *QuickBird* image of Xuzhou [RGB (R, G, B)]. (b) Reference image. (c)-(g) Classification maps produced by FCM, FCM_S1, FLICM AMASFC and FLDNICM, respectively.

In this experiment, a portion of 400×400 pixels of a multispectral QuickBird image is used, which was acquired in August 2005 (Fig. 13(a)) at a resolution of 0.61m×0.61m. The study area covers an urban area in Xuzhou City, China. Three multispectral bands (red, green, and blue) were used in this experiment. This region of the image was expected to contain five classes: road, bare soil, water, vegetation1 and vegetation2. The testing samples in the reference map (see Fig. 13(b)) were obtained combining the multispectral imagery with some fieldwork in September 2015. The parameters used in this experiment are $c=5$, $\varepsilon=1e-5$ and α=4.64 for FCM_S1.

The classification results of the five methods are shown in Fig. 13(c)-(g) provided by the FCM, FCM_S1, FLICM, AMASFC and FLDNICM algorithms which converged after 42, 73, 50, 47 and 45 iterations, respectively. The FCM result contains a lot of noise in the bare soil regions that are misclassified as road. FCM_S1 and AMASFC have close performance and both show a smaller amount of noise than FCM. However, many bare soil pixels are misclassified as road (see marked areas A and B). FLICM and FLDNICM are superior to the other three methods. Moreover, the inter-comparison between FLICM and FLDNICM reveals that the latter is better in persevering spatial details (such as thin features of the vegetation 1 class in area C and D).

Table VIII reports the quantitative results. As shown in the table, FCM_S1 and AMASFC have similar classification accuracies (the OA are all below 86%). FLDNICM produces an OA of 92.0%. The accuracy gains of FLDNICM over FCM, FCM_S1, FLICM and AMASFC are 13.21%, 8.88%, 4.50% and 6.35%, respectively.

TABLE VIII

COMPARISON OF PA, OA AND KC OF FIVE CLASSIFICATION METHODS (EXPERIMENT 3)

Class	Number of Testing samples	FCM	FCM_S1	FLICM	AMASFC	FLDNICM
Road	3405	89.54%	89.67%	91.51%	90.81%	88.69%
Bare soil	17831	61.67%	62.63%	77.28%	69.91%	85.30%
Water	4322	94.33%	94.15%	98.24%	93.48%	98.36%
Vegetation1	8013	53.39%	81.46%	86.57%	81.77%	92.31%
Vegetation2	19288	99.78%	99.13%	94.22%	99.16%	97.22%
OA		78.79%	83.12%	87.50%	85.65%	92.00%
KC		0.7117	0.7732	0.8309	0.8053	0.8903

E. Experiment 4: Salinas AVIRIS Image

In this experiment, a hyperspectral dataset was acquired by the AVIRIS sensor over the Salinas Valley, CA, USA [50]. The number of spectral bands is 204 and the used spatial size is 245×217. The spatial resolution is 3.7-m. Eight classes were identified in the area: Brocoli_green_weeds_2, Fallow, Fallow_smooth, Fallow_rough_plow, Stubble, Celery, Grapes_untrained and Vinyard_untrained. The testing samples is available online [50]. The parameters used in the five algorithms are $c=8$, $\varepsilon=1e-5$ and α=2.1 for FCM_S1. To reduce the computational complexity, the principal component analysis-based feature reduction was carried out, and the first ten components were used.

Fig. 14(c)-(g) shows the classification results provided by the FCM, FCM_S1, FLICM, AMASFC and FLDNICM algorithms which converged after 43, 46, 62, 75 and 81 iterations, respectively. Again, FLDNICM is visually more accurate than the other four methods. This can be illustrated by referring to marked areas A-D. As shown in Fig. 14(d), without considering any spatial information, a large amount of salt and pepper noise is present in the FCM result. Compared with FCM,

the local spatial constraints-based FCM methods produce more homogeneous and satisfactory results than FCM, In Fig. 14(d)-(f), some image details are lost. The reason may be that the central pixel is heavily influenced by its neighborhood pixels and its own information is not sufficiently accounted for in FCM_S1, FLICM and AMASFC. While the FLDNICM method obtains more homogeneous areas and preserves more image details than them. This is because the FLDNICM provides a more accurate trade-off between the central pixel and its neighboring pixels.

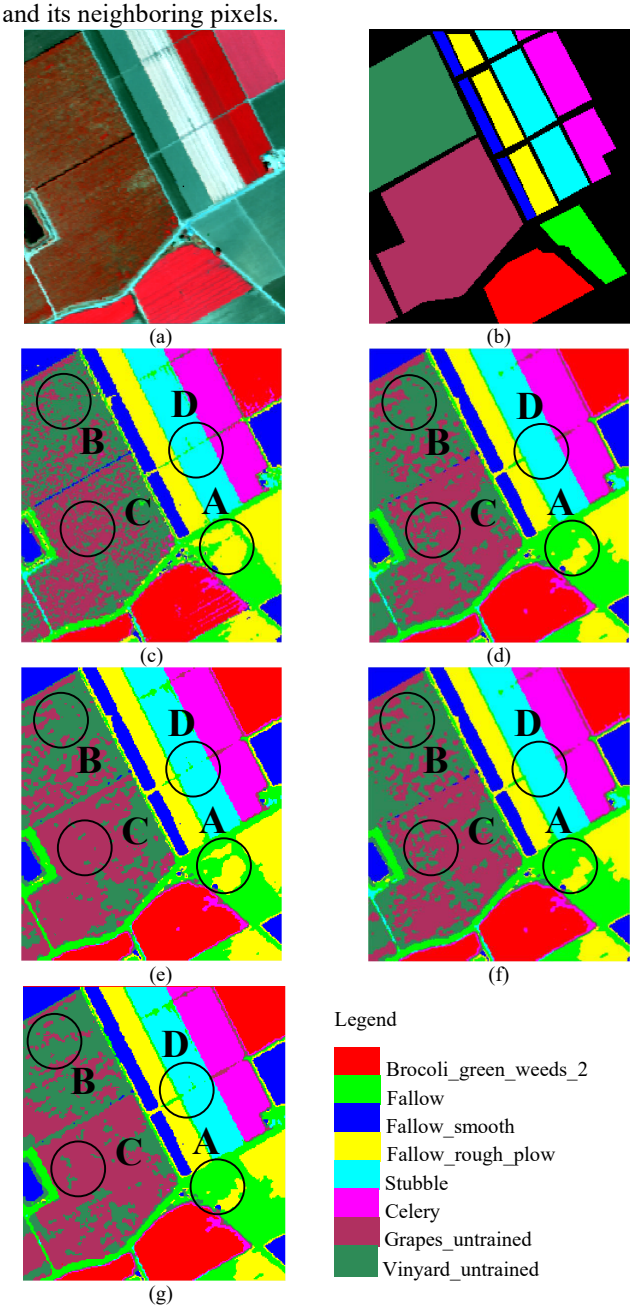

Fig. 14. Dataset and classification results in Experiment 4. (a) AVIRIS image of Salinas [RGB (70, 27, 17)]. (b) Reference image. (c)-(g) Classification maps produced by FCM, FCM_S1, FLICM, AMASFC and FLDNICM, respectively.

The quantitative evaluation results are list in Table IX. As seen from Table IX, the local spatial constraints based-algorithms all yield greater OA than FCM, and FLDNICM produces the greatest Overall Accuracy (84.46%), with gains of 8.37%, 5.95%, 4.43% and 4.83% over FCM, FCM_S1, FLICM and AMASFC, respectively.

TABLE IX

COMPARISON OF PA, OA AND KC OF FIVE CLASSIFICATION METHODS (EXPERIMENT 4)

Class	Number of Testing samples	FCM	FCM_S1	FLICM	AMASFC	FLDNICM
Brocoli_green_weeds_2	3563	92.17%	95.50%	96.15%	95.76%	97.76%
Fallow	1976	52.52%	55.51%	67.11%	83.42%	87.35%
Fallow_rough_plow	1394	99.58%	99.45%	98.49%	97.63%	99.86%
Fallow_smooth	2678	97.60%	95.30%	94.36%	88.84%	93.99%
Stubble	3959	98.10%	99.64%	97.75%	99.85%	97.90%
Celery	3579	99.01%	98.96%	99.02%	98.84%	98.83%
Grapes_untrained	11231	56.94%	60.78%	70.14%	60.40%	78.12%
Vinyard_untrained	7268	68.51%	72.03%	63.11%	73.07%	67.05%
OA		76.09%	78.51%	80.03%	79.63%	84.46%
KC		0.7101	0.7391	0.7562	0.7576	0.8098

F. Analysis of the Computational Complexity

All the four images are used to test the computational time of the proposed FLDNICM technique and of other FCM-based algorithms. All techniques were tested on an Intel Xeon ® CPU X5675 at 3.06-GHz, each algorithm is run ten times on each test image and the average times are provided. Table X shows the average computational time for the five methods. As one can see, the FLDNICM takes the largest time for each image, as weightings and effects on the central pixel from its neighboring pixels should be calculated at each iteration. However, this increase of computational load results in a significant increase of the classification accuracy.

TABLE X

AVERAGE COMPUTATIONAL TIME OF FLDNICM AND OTHER FCM RELATED METHODS (SECONDS)

No.	Number of class	Image size	FCM	FCM_S1	FLICM	AMASFC	FLDNICM
1	4	165×272×6	1.68	4.75	18.43	19.14	20.61
2	4	400×400×4	3.26	11.07	60.02	80.08	90.77
3	5	512×512×3	7.01	21.86	118.75	129.34	138.37
4	8	245×217×10	2.53	9.91	57.81	81.65	90.22

V. CONCLUSION

In this paper a FLDNICM clustering algorithm for remotely sensed imagery classification has been proposed. The proposed algorithm can overcome the drawbacks of the well-known FCM by incorporating local spatial and gray level information. The FLDNICM is effective in removing noise pixels and reducing the edge blurring artifacts simultaneously. This advantage is due to the introduced trade-off weighted fuzzy factor and fuzzy prior probability function, which can provide accurate trade-off weighted factors between the central pixel and its neighboring pixels. This makes FLDNICM both more robust to outliers and effective in preserving details in relatively strong noisy environment when compared to other FCM with spatial variants. Experiments on three different remotely sensed imagery datasets and a gray image with mixed noise are conducted to demonstrate the effectiveness of

FLDNICM. Compared with existing FCM, FCM_S1, FLICM, AMASFC and FLDNICM resulted more accurate both in visual and quantitative evaluation for most classes. Therefore, FLDNICM is an effective unsupervised classifier for remotely sensed imagery.

In further studies, additional research will be conducted on the selection of the initial cluster centers, determining the cluster number and reducing the computational cost.

ACKNOWLEDGMENT

The authors would like to thank the Editor, Associate Editor, and anonymous reviewers for their helpful comments and suggestions that improved this paper.

REFERENCES

[1] D. Lu and Q. Weng, "A survey of image classification methods and techniques for improving classification performance," *Int. J. Remote Sens*., vol. 28, no. 5, pp. 823-870, Mar. 2007.

[2] P. R. Kersten, J. S. Lee, and T. L. Ainsworth, "Unsupervised classification of polarimetric synthetic aperture radar images using fuzzy clustering and EM clustering," *IEEE Trans. Geosci. Remote Sens.*, vol. 43, no. 3, pp. 519–527, Mar. 2005.

[3] C. C. Hung, S. Kulkarni and B. C Kuo, "A new weighted fuzzy *c*-means clustering algorithm for remotely sensed image classification," *IEEE Trans. Geosci. Remote Sens.*, vol. 5, no. 3, pp. 543–553, June. 2011.

[4] N. B. Venkateswarlu and P.S.V.S.K. Raju," Fast isodata clustering algorithms," *Pattern Recognit.*, vol. 25, no, 3, pp. 335-342, Mar. 1992.

[5] K. Xu *et al.*, "Unsupervised satellite image classification using markov field topic model," *IEEE Geosci. Remote Sens. Lett.*, vol. 10, no. 1, pp. 130–134, Jan. 2013.

[6] E. Blanzieri and F. Melgani, "Nearest neighbor classification of remote sensing images with the maximal margin principle," *IEEE Trans. Geosci. Remote Sens.,* vol. 46, no. 6, pp. 1804–1811, Jun. 2008.

[7] J. C. Dunn, "A fuzzy relative of the ISODATA process and its use in detecting compact well-separated clusters," *Journal of Cybernetics*, vol. 3, no. 3, pp. 32-57. 1973.

[8] J. C. Bezdek, *Pattern Recognition with Fuzzy Objective Function Algorithms*. New York, NY, USA: Plenum, 1981.

[9] S. Krinidis and V. Chatzis, "A robust fuzzy local information *c*-means clustering algorithm," *IEEE Trans. Image Process*., vol. 19, no. 5, pp. 1328–1337, May 2010.

[10] Z. Ji, J Liu, G Cao, Q Sun and Q Chen, "Robust spatially constrained fuzzy *c*-means algorithm for brain MR image segmentation," *Pattern Recognit*., vol. 47, no. 7, pp. 2454–2466, July. 2014.

[11] J. Udupa and S. Samarasekera, "Fuzzy connectedness and object definition: theory, algorithm and applications in image segmentation," *Graph. Models Image Process*., vol. 58, no. 3, pp. 246–261, May. 1996.

[12] R. Shang et al., "A spatial fuzzy clustering algorithm with kernel metric based on immune clone for SAR image segmentation," *IEEE J. Sel. Topics Appl. Earth Observ. Remote Sens.,* vol. 9, no. 4, pp. 1640–1652, Apr. 2016.

[13] M. N. Ahmed et al., "A modified fuzzy *c*-means algorithm for bias field estimation and segmentation of MRI data," *IEEE Trans. Med. Imag*., vol. 21, no. 3, pp. 193–199, 2002. Mar. 2002.

[14] W. Cai, S. Chen, and D. Zhang, "Fast and robust fuzzy *c*-means clustering algorithms incorporating local information for image segmentation," *Pattern Recognit*., vol. 40, no. 3, pp. 825–838, Mar. 2007.

[15] Z. Wang et al., "Adaptive spatial information-theoretic clustering for image segmentation," *Pattern Recognit*., vol. 42, no. 9, pp. 2029–2044, Sep. 2009.

[16] S. Ghaffarian and S. Ghaffarian, "Automatic histogram-based fuzzy C-means clustering for remote sensing imagery," *ISPRS J. Photogramm. Remote Sens*., vol. 97, pp. 46-57, Nov. 2014.

[17] H. Verma, R. K. Agrawal and A. Sharan, "An improved intuitionistic fuzzy c-means clustering algorithm incorporating local information for brain image segmentation," *Appl Soft Comput*., vol. 46, pp. 543–557, Sep. 2016.

[18] Q. Zhao et al., "A fuzzy clustering image segmentation algorithm based on Hidden Markov Random Field models and Voronoi Tessellation," *Pattern Recongn Lett.*, vol. 85, no. 1, pp. 49–55, Jan. 2017.

[19] M. Gong et al., "Change detection in synthetic aperture radar images based on image fusion and fuzzy clustering," *IEEE Trans. Image Process*., vol. 21, no. 4, pp. 2141–2151, May. 2012.

[20] M. Gong et al., "Fuzzy *c*-means clustering with local information and kernel metric for image segmentation," *IEEE Trans. Image Process*., vol. 22, no. 2, pp. 573–584, Feb. 2013.

[21] N. Li et al., "A spatial clustering method with edge weighting for image segmentation," *IEEE Geosci. Remote Sens. Lett.*, vol. 10, no. 5, pp. 1124–1128, Sep. 2013

[22] X. Bai et al., "Infrared ship target segmentation based on spatial information improved FCM," *IEEE Tran. Cybern*., vol. 46, no. 12, pp. 3259–3271, Dec. 2016.

[23] X. Yu et al., "Land cover classification of remote sensing imagery based on interval-valued data fuzzy c-means algorithm," *Sci China Earth Sci.*, vol. 57, no. 6, pp. 1306-1313, 2013.

[24] J. Ji and K. L. Wang, "A robust nonlocal fuzzy clustering algorithm with between-cluster separation measure for SAR image segmentation," *IEEE J. Sel. Topics Appl. Earth Observ. Remote Sens.*, vol. 7, no. 12, pp. 4929-4936, Dec. 2014

[25] Y. Zhong et al., "An adaptive memetic fuzzy clustering algorithm with spatial information for remote sensing imagery," *IEEE J. Sel. Topics Appl. Earth Observ. Remote Sens.*, vol. 7, no. 4, pp. 1235-1248, Apr. 2014.

[26] I. Dópido et al., "A quantitative and comparative assessment of unmixing-based feature extraction techniques for hyperspectral image classification," *IEEE J. Sel. Topics Appl. Earth Observ. Remote Sens.,* vol. 5, no. 2, pp. 421-435, Apr. 2012.

[27] Q. Wang and W Shi, "Unsupervised classification based on fuzzy c-means with uncertainty analysis," *Remote Sens Lett.*, vol. 4, no. 11, pp. 1087–1096, Nov. 2013

[28] M. N. Ahmed, S.M. Yamany, A.A. Farag, T. Moriaty, Bias field estimation and adaptive segmentation of MRI data using a modified fuzzy c-means algorithm, in: Proceedings of the 13th International Conference on Computer Assisted Radiology and Surgery, CARS'99, Paris, 1999, p. 1004.

[29] D. L. Pham, "Spatial models for fuzzy clustering," *Comput Vis Image Underst*, vol. 84, no. 2, pp. 285-297, Nov. 2001.

[30] S. Chen and D. Zhang, "Robust image segmentation using FCM with spatial constraints based on new kernel-induced distance measure," *IEEE Trans. Syst., Man, Cybern.*, vol. 34, no. 4, pp. 1907–1916, Aug, 2004

[31] L. Szilagyi *et al.*, "MR brain image segmentation using an enhanced fuzzy *c*-means algorithm," in *Proc. 25th Annu. Int. Conf. IEEE EMBS*, 2003, pp. 17–21.

[32] X. Wang, X. Lin and Z. Yuan, "An edge sensing fuzzy local information *c*-means clustering algorithm for image segmentation" in Lecture Notes in Computer Science, vol. 8589, Intelligent Computing Methodologies, D.S. Huang et al, Ed. 2014, pp. 230–240.

[33] J. Yu, Q. Cheng and H. Huang, "Analysis of the weighting exponent in the FCM," *IEEE Trans. Syst. Man, Cybern. B*, vol. 34, no. 1, pp. 634-639, Feb. 2004.

[34] G. Sun et al., "A novel approach for edge detection based on the theory of universal gravity," *Pattern Recognit.*, vol. 40, no. 10, pp. 2766–2775, Oct. 2007.

[35] K. C. Mertens et al., "A sub-pixel mapping algorithm based on sub-pixel/pixel spatial attraction models," *Int. J. Remote Sens*., vol. 27, no. 15, pp. 3293-3310, Aug. 2006.

[36] S. Z. Li, *Markov Random Field Modeling in Image Analysis*. New York: Springer-Verlag, 2010.

[37] H. Yang et al., "Remote sensing classification using fuzzy *c*-means clustering with spatial constraints based on markov random field," *EUR J REMOTE SENS*., vol. 46, no. 15, pp. 305-316, Aug. 2013.

[38] Y. Tarabalka, M. Fauvel and J. Chanussot, "SVM- and MRF-based method for accurate classification of hyperspectral images," *IEEE Geosci. Remote Sens. Lett.*, vol. 7, no. 4, pp. 736-740, Oct, 2010.

[39] B. Zhang et al., "Adaptive markov random field approach for classification of hyperspectral imagery," *IEEE Geosci. Remote Sens. Lett.*, vol. 8, no. 5, pp. 973-977, Sep. 2011.

[40] A. H. S. Solberg, T. Taxt and A. K. Jain, "A Markov random field model for classification of multisource satellite imagery," *IEEE Trans. Geosci. Remote Sens*., vol. 34, no. 1, pp. 100-113, Jan. 1996.

[41] R. G. Congalton, R. G. Oderwald and R. A. Mead, "Assessing landsat classification accuracy using discrete multivariate statistical techniques," *Photogramm. Eng. Remote Sens*., Vol. 49, no. 12, pp. 1671-1678, Dec. 1983.
[42] J. C. Bezdek, "Numerical taxonomy with fuzzy sets," *J. Math. Biol*., vol. 1, no. 1, pp. 57-71, May. 1974.
[43] J. C. Bezdek, "Cluster validity with fuzzy sets, " *J. Cybernet*., vol. 3, no. 3, pp. 58-73, 1973.
[44] R. N. Dave, "Validating fuzzy partitions obtained through *c*-shells clustering," *Pattern Recongn Lett.*, vol. 17, no. 6, pp. 613-623, May. 1996.
[45] Y. Fukuyama and M. Sugeno, "A new method of choosing the number of clusters for the fuzzy *c*-means method,". in: Proceedings of Fifth Fuzzy Systems Symposium, pp. 247-250, Jan. 1989.
[46] X. Xie and G. Beni, "A validity measure for fuzzy clustering," *IEEE Trans. Pattern Anal. Mach. Intell*., vol. 13, no. 8, pp. 841-847, Aug. 1991.
[47] S. H. Kwon, "Cluster validity index for fuzzy clustering," *Electron. Lett.*, vol. 34, no. 22, pp. 2176-2177, Oct. 1998.
[48] Y. Tang, F. Sun and Z. Sun, "Improved validation index for fuzzy clustering," in: American Control Conf., June 8-10, 2005, Portland, OR, USA.
[49] K. Wu and M. Yang, "A cluster validity index for fuzzy clustering," *Pattern Recongn Lett.*, vol. 26, no. 9, pp. 1275-1291, Jul. 2005.
[50] [Online].Available:http://www.ehu.eus/ccwintco/index.php/Hyperspectral_Remote_Sensing_Scenes

Hua Zhang is an associate Professor in GIS and remote sensing, Key Laboratory for Land Environment and Disaster Monitoring of SBSM, China University of Mining and Technology. He obtained his doctoral degree from China University of Mining and Technology, Xuzhou, China in 2012. He has authored or coauthored over 20 peer-reviewed articles in international journals such as *IEEE Transactions on Geoscience and Remote Sensing*, and *ISPRS Journal of Photogrammetry and Remote Sensing*. His current research interests include multi/hyperspectral and high-resolution remotely sensed images processing, uncertainty in classification, pattern recognition, and remote sensing applications. He was a recipient of the Excellent Doctoral Dissertation Award and the Excellent Graduates in Jiangsu Province, China, in 2012.

Lorenzo Bruzzone (S'95–M'98–SM'03–F'10) received the Laurea (M.S.) degree in electronic engineering (*summa cum laude*) and the Ph.D. degree in telecommunications from the University of Genoa, Genoa, Italy, in 1993 and 1998, respectively. He is currently a Full Professor of Telecommunications with the University of Trento, Trento, Italy, where he teaches remote sensing, radar, pattern recognition, and electrical communications. He is also the Founder and the Director of the Remote Sensing Laboratory with the Department of Information Engineering and Computer Science, University of Trento. He is the Principal Investigator of the Radar for Icy Moon Exploration Instrument in the framework of the JUpiter ICy Moons Explorer Mission of the European Space Agency. His research interests include remote sensing, radar and SAR, signal processing, and pattern recognition. He promotes and supervises research on these topics within the frameworks of many national and international projects.

Dr. Bruzzone has been a member of the Administrative Committee of the IEEE Geoscience and Remote Sensing Society since 2009. He was a Guest Co-Editor of different Special Issues of international journals. He is the Co-Founder of the IEEE International Workshop on the Analysis of MultiTemporal Remote-Sensing Images (MultiTemp) series and is currently a member of the Permanent Steering Committee of this series of workshops. Since 2003, he has been the Chair of the SPIE Conference on Image and Signal Processing for Remote Sensing. Since 2013, he has been the Founder Editor-in-Chief of the IEEE GEOSCIENCE AND REMOTE SENSING MAGAZINE. Currently, he is an Associate Editor of the IEEE TRANSACTIONS ON GEOSCIENCE AND REMOTE SENSING and the *Journal of Applied Remote Sensing*. He was invited as a Keynote Speaker in 30 international conferences and workshops. Since 2012, he has been a Distinguished Speaker of the IEEE Geoscience and Remote Sensing Society.

Wenzhong Shi is a Professor in GIS and remote sensing, Department of Land Surveying and Geo-Informatics, the Hong Kong Polytechnic University. He obtained his doctoral degree from University of Osnabrück in Vechta, Germany in 1994. His current research interests include GIS and remote sensing, uncertainty and spatial data quality control, image processing for high resolution satellite images. He has published some 400 research articles (including over 100 SCI papers) and 10 books. He received the State Natural Science Award from the State Council of China in 2007 and The Wang Zhizhuo Award from International Society for Photogrammetry and Remote Sensing in 2012.

Ming Hao is a postdoctoral researcher at the School of Environmental Science and Spatial Informatics, China University of Mining and Technology. He received his Doctoral degree in China University of Mining and Technology in 2015, China. He has authored or coauthored over 10 peer-reviewed articles in international journals such as *Remote Sensing, International Journal of Remote Sensing and IEEE Geoscience and Remote Sensing Letters.* His research interests include image processing, information extraction from remote sensing images and remote sensing image fusion.

Yun Jia Wang received the M.Eng. degree in mine surveying and the Ph.D. degree in mining engineering from the China University of Mining and Technology, Xuzhou, China, in 1988 and 2000, respectively. From 2002 to 2004, he was a Post-Doctoral Fellow with the China University of Mining and Technology. He joined the Royal Melbourne Institute of Technology, Melbourne, Australia, as a Visiting Research Scholar in 2006, and the Ryerson University, Toronto, ON, Canada, in 2014. He is currently a Full Professor and the Dean with the School of Environmental Science and Spatial Informatics, China University of Mining and Technology. His research interests include ubiquitous positioning and navigation, mine disaster monitoring, and carbon emission/sink monitoring.